

Validation of Aura Microwave Limb Sounder OH and HO₂ Measurements

H. M. Pickett, B. J. Drouin, T. Canty, R. J. Salawitch, R. A. Fuller, V. S. Perun, N. J. Livesey, J. W. Waters, R. A. Stachnik, S. P. Sander, and W. A. Traub

Jet Propulsion Laboratory, Calif. Inst. of Tech., Pasadena, California, USA

K. W. Jucks

Harvard-Smithsonian Center for Astrophysics, Cambridge, Massachusetts, USA

K. Minschwaner

New Mexico Institute of Mining and Technology, Socorro, New Mexico, USA

Abstract.

The Microwave Limb Sounder (MLS) instrument on the Aura satellite obtains global measurements of both OH and HO₂ radicals. This paper describes the precision and systematic errors of the MLS version v2.2 of the retrieval software. Estimated systematic errors are less than 8% for OH over 32-0.003 hPa and HO₂ over 6.8-0.21 hPa. Comparison of measurements from MLS OH and HO₂ profiles and 3 balloon-based instruments show good agreement among themselves and with a photochemical model using standard chemistry (i.e. recommended rate constants). Similarly, good agreement is seen between column OH found by integrating satellite profiles and ground-based measurements of column OH. The agreement between measured and modeled OH and HO₂ is improved following perturbations to the rate constants O+OH and OH+HO₂ that are within the recommended uncertainties. Measurements of OH obtained a decade ago by the Middle Atmosphere High Resolution Spectrograph Investigation (MAHRSI) are smaller than MLS measurements by 20% at 70 km, are similar to MLS data near 50 km, and are 50% larger than MLS observations near 42 km. The MLS and MAHRSI measurements of OH overlap at the limit of their respective 2- σ uncertainties. Most importantly, we find the shape of the OH profile measured by MLS is simulated well using standard chemistry.

Introduction

The Aura satellite was launched on July 15, 2004 into a sun-synchronous near-polar orbit. The Microwave Limb Sounder (MLS) instrument on the Aura satellite measures the hydroxyl radical (OH) and the peroxy radical (HO₂) both day and night [Waters *et al.*, 2006]. Details on the THz module that measures OH and its calibration are given in Pickett [2006a]. Details on the retrieval algorithms are given by Livesey *et al.*

[2006]. Early validation of OH and HO₂ with balloon-borne remote sensing instruments is given in Pickett, *et al* [2006b]. Early validation of other molecules measured by MLS is given in Froidevaux *et al.* [2006]. The current version of the MLS retrieval software is v2.2 and is the current production software. All the data taken from launch to February 2007 has been processed with the earlier version v1.5. The data since launch will be reprocessed with version v2.2, but only selected

days have been reprocessed thus far. However, unless otherwise stated, this paper will use version v2.2. A description of the differences between these two major versions as it relates to HO_x will be given below.

Odd hydrogen (HO_x=OH+HO₂+H) chemistry dominates atmospheric ozone destruction at heights above 40 km [Osterman, *et al.*, 2005] and below 22 km [Salawitch, *et al.*, 2005]. Observations of OH over 40–80 km from the Middle Atmosphere High Resolution Spectrograph Investigation (MAHRSI) [Conway *et al.*, 2000] were not consistent with standard chemistry (JPL recommended rates). Photochemical models could not reconcile with MAHRSI data over 40–80 km using adjusted rate constants for known reactions. Changes needed to fix the mesospheric OH made the situation worse at 40 km, leading to the designation “HO_x dilemma.” However, balloon-borne observations that are mostly sensitive to HO_x below 40 km agree better with photochemical theory [Jucks *et al.*, 1998] and with MLS measurements of HO_x [Canty *et al.*, 2006].

MLS Measurements

Overview

The Aura satellite was launched on 15 July 2004 into a sun synchronous orbit with a 13.75 hr ascending node equatorial crossing. The Microwave Limb Sounder is one of four instruments included on the satellite. For latitudes near 34°N, the MLS overpass occurs at 13.5 hr local solar time (LST) and again at 2.5 hr LST. At latitudes above 70° up to the orbital-inclination limit of 83°, the MLS overpass LST changes rapidly. MLS scans vertically in the plane of the orbit. Consequently, the longitude of the MLS footprint changes by 24° each orbit. For consistency with other measurements on MLS, retrieved profiles are archived in volume mixing ratio units on pressure surfaces with 6 / decade vertical resolution.

The OH measurements are made with a THz receiver [Pickett, 2006a] that uses a gas laser as the local oscillator [Mueller *et al.*, 2007]. There are six receiver bands (15–20) in the THz receiver, each connected to a 25-channel filter-bank. The filters near the center of each band are 6 MHz wide, and the width increases to 96 MHz at ± 575 MHz from band center. Four of these bands (15,16,18,19) are used to observe OH. In addition there are two receiver bands (17,20) that are used for pointing information. The frequencies of the target lines are shown in Table 1 and an example of the observed radiance is shown in Figure 1.

The OH lines indicated in Table 1 are each split into

3 hyperfine components [Blake *et al.*, 1986]. There are two THz mixers, one for each of two different linear polarizations, that provide simultaneous measurements to improve the OH signal to noise ratio. Bands 15–17 and bands 18–20 have perpendicular polarizations, with axes that are oriented $\sim 26^\circ$ from nadir. The Zeeman splitting is $\sim \pm 1$ MHz and, in the small splitting limit, the polarization differences can be shown to be proportional to the square of the ratio of the Zeeman shift to the Doppler width (6 MHz). Therefore, measurements from the two polarizations are fitted simultaneously by a model of unpolarized emission. Bands 16 and 19 have an O₃ line at the edge from which an O₃ profile is retrieved. While the noise associated with the THz O₃ profile is large compared with the O₃ profile from the GHz bands, comparison of the THz profile with GHz O₃ gives added information on systematic errors.

Table 1. Target molecule line-center frequencies for MLS HO_x bands

Band	Molecule	Frequency / GHz
15, 18	OH	2514.317
16, 19	OH	2509.949
16, 19	O ₃	2509.560
17, 20	O ₂	2502.324
17, 20	O ₃	2543.208
28	HO ₂	649.702
30	HO ₂	660.486

The THz module retrieves pointing information from bands 17 and 20 using a magnetic dipole line of O₂ in the lower sideband and a strong line of O₃ in the upper sideband. Band 20 does not have a dedicated filter bank, but the filter-bank used nominally for 640-GHz N₂O can be switched to band 20. During instrument check out shortly after launch, the band 20 performance was measured and bore-sight offsets were determined. Since then the instrument has been configured for N₂O measurements and band 20 data is not available. An example of the observed band 17 radiance is shown in Figure 2.

The HO₂ measurements are made from two HO₂ lines in the 640 GHz radiometer each using a 11-channel mid-band filter-bank. These filter-banks are identical in design to the center channels of the standard 25-channel filter-bank and are embedded in the frequency space of other bands. Data from all the filter-banks in the 640 GHz radiometer are used to retrieve profiles for eight other molecules in addition to HO₂. An example of the observed radiance is shown in Figure 3. The HO₂ signal is only ~ 1 K and signal / noise is ~ 3 after

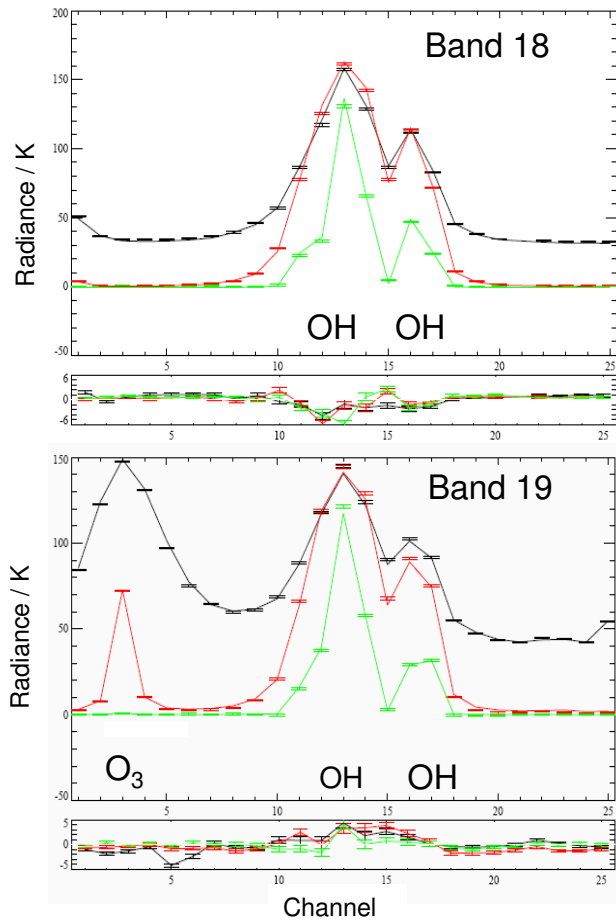


Figure 1. MLS radiance and residuals for Bands 18 and 19. The OH emission shown here is composed of 3 hyperfine components. Radiance is a daylight zonal average over latitudes from 60S to 60N for 28 January 2005. The radiance is nearly identical for Bands 15 and 16. The horizontal axis is the filter-bank channel number. The vertical axis is radiance in K. The black, red, and green plots are for tangent heights of 31.5, 40.7, and 62.5 km, respectively. The solid lines in the large panels are the predicted radiance and the center point of the error bars indicate the observed radiance. The small panels show the residuals for the observed minus calculated radiance.

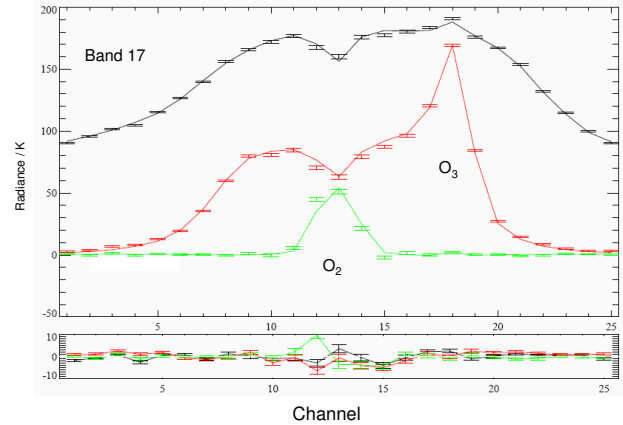


Figure 2. MLS radiance and residuals for Band 17. The O₂ emission is in the lower sideband and the THz O₃ emission is in the upper sideband. This band provides pointing information. Radiance shown here is a daylight zonal average over latitudes from 60S to 60N on 28 January 2005. See Figure 1 for further details.

a zonal average over 120° latitude. Consequently, 12 days of data are needed to obtain a zonal mean over a 10° latitude range with the same signal/noise as shown in the figure.

A day–night HO₂ difference is required to reduce systematic errors to an acceptable level. The actual radiances in band 28 and 30 corresponding to the differences shown in Figure 3 are quite large due in part to absorption by ozone. In band 28 at 40 km tangent height the background radiance is 25 K, while for band 30 the radiance changes from 50 K to 100 K across the band. The day–night differencing works for pressures above 0.03 hPa. Below this pressure there can be significant HO₂ at night due to the long reactive lifetimes of HO_x at these low pressures [Pickett *et al.*, 2006c], but use of data below this pressure is also not recommended because of undue influence of a priori profiles.

The MLS Level 2 data (retrieved geophysical parameters and diagnostics at the measurement locations along the suborbital track) are generated from input Level 1 data (calibrated radiances and engineering information) by the MLS data processing software. The MLS retrieval algorithms, described in detail by Livesey *et al.* [2006], are based on the standard optimal estimation method. They employ a two-dimensional approach that takes into account the fact that limb observations from consecutive scans cover significantly overlapping regions of the atmosphere. The results are reported in Level 2 Geophysical Product

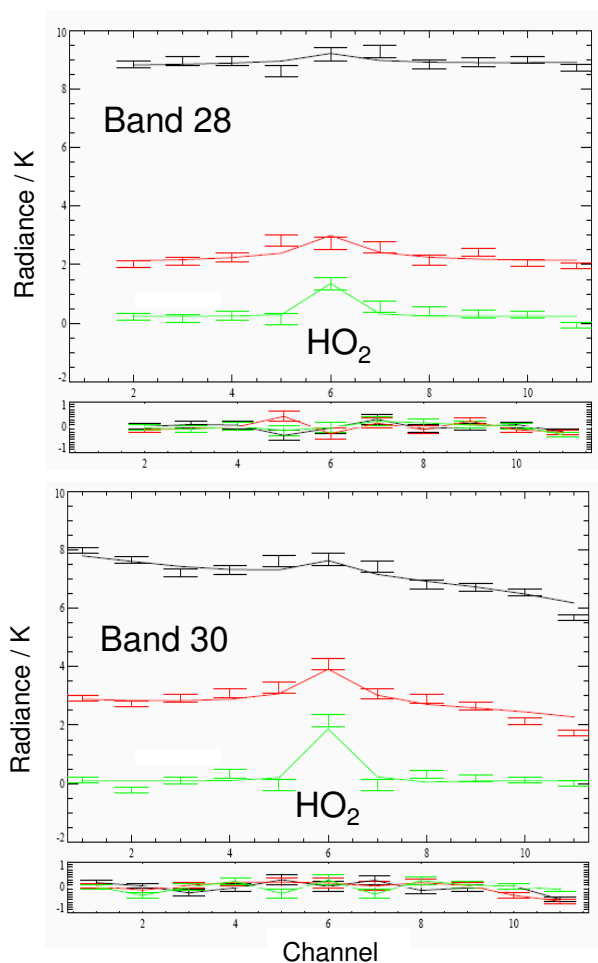


Figure 3. MLS radiance and residuals for Bands 28 and 30. The radiance shown is a day-night difference of zonal averages for latitudes from 60S to 60N on 28 January 2005. See Figure 1 for further details.

(L2GP) files, which are standard HDF-EOS version 5 files containing swaths in the Aura-wide standard format [Livesey *et al.*, 2007, available from the MLS web site, <http://mls.jpl.nasa.gov>]. A separate L2GP file is produced for each standard MLS product for each day (00–24 UT).

Data Screening

Examples of the THz spectra and residuals for daytime are shown in Figures 1 and 2. To obtain radiance closure such as that shown in the Figures, it is essential to screen the data using 3 pieces of information from the L2GP swath structure:

1. Use only even values of STATUS. Profiles with odd STATUS are flagged by the level 2 retrieval software for various errors that are described by other bits in the STATUS word (see Table 2).
2. Use only positive precision values. The precision field is flagged by the level-2 software with a negative sign when the estimated precision is 50% of the a priori precision. Negative precisions usually appear at the edge of the useful pressure range.
3. Use only scans with CONVERGENCE < 1.1. This field contains additional information on the success of the retrieval and compares the fit profiles to that expected by the linearized retrieval, with values around 1.0 typically indicating good convergence. A cutoff of 1.1 is a compromise between eliminating pathological non-converging fits and keeping fits that have adequately converged.

For some seasons, the Gas Laser Local Oscillator (GLLO) for the THz receiver is automatically relocked as many as 5 times during a day. These relock events occur when the tuning range of the laser is less than the thermal excursion over an orbit and over a day. This thermal effect depends on the albedo of the Earth as seen by the GLLO radiator. In these cases the status flag is 257 and the profile is ignored. This is only a problem for mapping because the missing data may appear at the same latitude and longitude on successive days.

Over the pressure range of 32–10 hPa, one should use day–night differences to reduce biases. The recommended range for OH is 32–0.003 hPa.

An example of the spectra and residuals in the 640 GHz radiometer near the two HO₂ lines are shown in Figure 3. The radiance shown is a day–night difference. The data filtering procedure is identical to that

Table 2. Meaning of bits in the ‘Status’ field.

Bit	Value ^a	Meaning
0	1	Flag: Do not use this profile (see bits 8–9 for details)
1	2	Flag: This profile is ‘suspect’ (see bits 4–6 for details)
2	4	Unused
3	8	Unused
4	16	Information: This profile may have been affected by high altitude clouds
5	32	Information: This profile may have been affected by low altitude clouds
6	64	Information: This profile did not use GEOS-5 temperature a priori data
7	128	Unused
8	256	Information: Retrieval diverged or too few radiances available for retrieval
9	512	Information: The task retrieving data for this profile crashed (typically a computer failure)

^a ‘Status’ field in L2GP file is total of appropriate entries in this column.

for the THz OH retrievals. Recommended range for HO₂ is 21–0.03 hPa

Resolution and Precision

The resolution of the retrieved profiles is described by the averaging kernels. Because the level 2 processing uses a 2-dimensional retrieval, the averaging kernel has both a vertical component and a horizontal component in the direction of the line of sight. Perpendicular to the line of sight the spatial resolution is determined by the horizontal width of the antenna pattern and is 1.5 km (HO₂) to 2.5 km (OH).

Figure 4 shows typical two-dimensional (vertical and horizontal along-track) averaging kernels for the MLS v2.2 OH data at 70°N. Variation in the averaging kernels is sufficiently small that these are representative for all profiles. Colored lines show the averaging kernels as a function of MLS retrieval level, indicating the region of the atmosphere from which information is contributing to the measurements on the individual retrieval surfaces, which are denoted by plus signs in corresponding colors. The dashed black line indicates the resolution, determined from the full width at half maximum (FWHM) of the averaging kernels, approximately scaled into kilometers (top axis). The top panel of Figure 4 shows vertical averaging kernels (integrated in the horizontal dimension for 5 along-track scans) along with the resolution (dashed line). The solid black line shows the integrated area under each kernel (horizontally and vertically). Values near unity imply that the majority of information for that MLS data point has come from the measurements, whereas lower values imply substantial contributions from a priori information. The bottom panel of Figure 4 shows horizontal averaging kernels (in-

tegrated in the vertical dimension) along with the resolution (dashed line). The averaging kernels are scaled such that a unit change is equivalent to one decade in pressure. The vertical width of the averaging kernel at pressures above 0.01 hPa is 2.5 km. The horizontal width of the averaging kernel is equivalent to a width of 1.5° (165 km) distance along the orbit and is equivalent to one scan interval (24.67 s). The changes in vertical resolution below pressures below 0.01 hPa are due mainly to use of a faster operational scan rate for tangent heights above 70 km.

Figure 5 shows typical two-dimensional (vertical and horizontal along-track) averaging kernels for the MLS v2.2 HO₂ data at 70°N. Details about the Figure and associated averaging kernel are the same as OH given above. The vertical width of the averaging kernel at pressures above 0.1 hPa is 4 km. The horizontal width of the averaging kernel is 2–4 profiles or a 3–6° distance along the orbit. In software version v2.2, smoothing of the profile was applied to reduce indeterminacy in the fit that was manifested in v1.5 as a vertical oscillation in the profile. The effect of the smoothing in v2.2 is to broaden the vertical averaging kernels to a width of 4 km and to broaden the horizontal averaging kernel by a factor of 2–4.

A typical OH concentration profile and associated precision estimate is shown in Figure 6. The profile is shown both in volume mixing ratio (vmr) and density units. All MLS data are reported in vmr for consistency with the other retrieved molecular profiles. However, use of density units (10⁶ cm^{−3}) reduces the apparent steep vertical gradient of HO_x allowing one to see the profile with more detail. Additionally, at THz frequencies the collisional line-width is approximately equal to

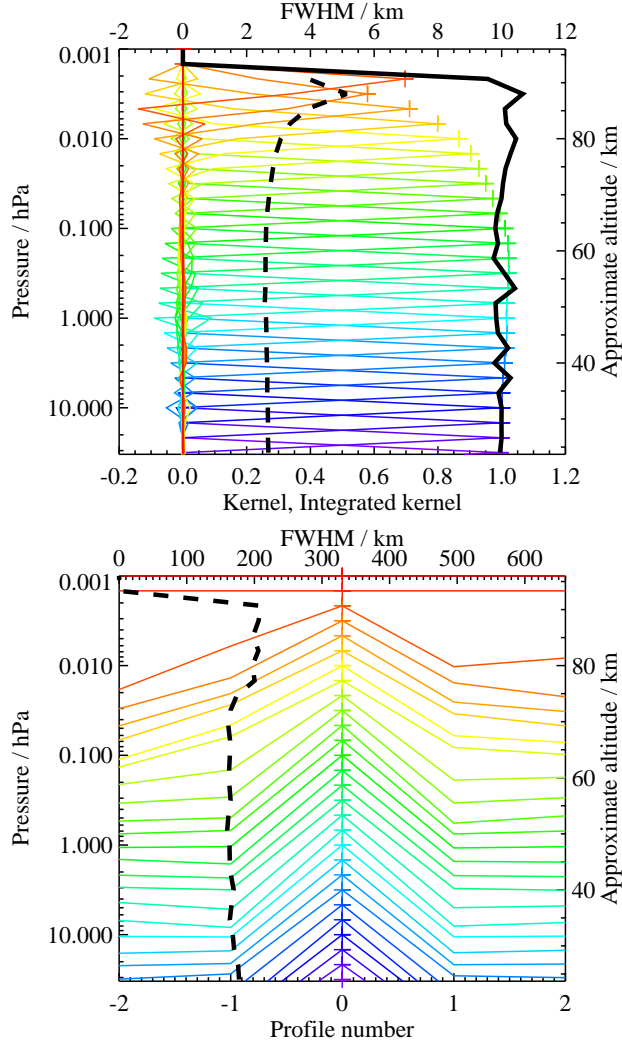


Figure 4. Typical two-dimensional (vertical and horizontal along-track) averaging kernels for the MLS v2.2 OH data at 70°N. Vertical averaging kernels for OH are shown in the upper panel. The lower panel shows the horizontal averaging kernels along the line of sight. The individual colored plots are the averaging kernels. The dashed black line is the width of the kernel (top axes) and the solid black line is its integral (bottom axes).

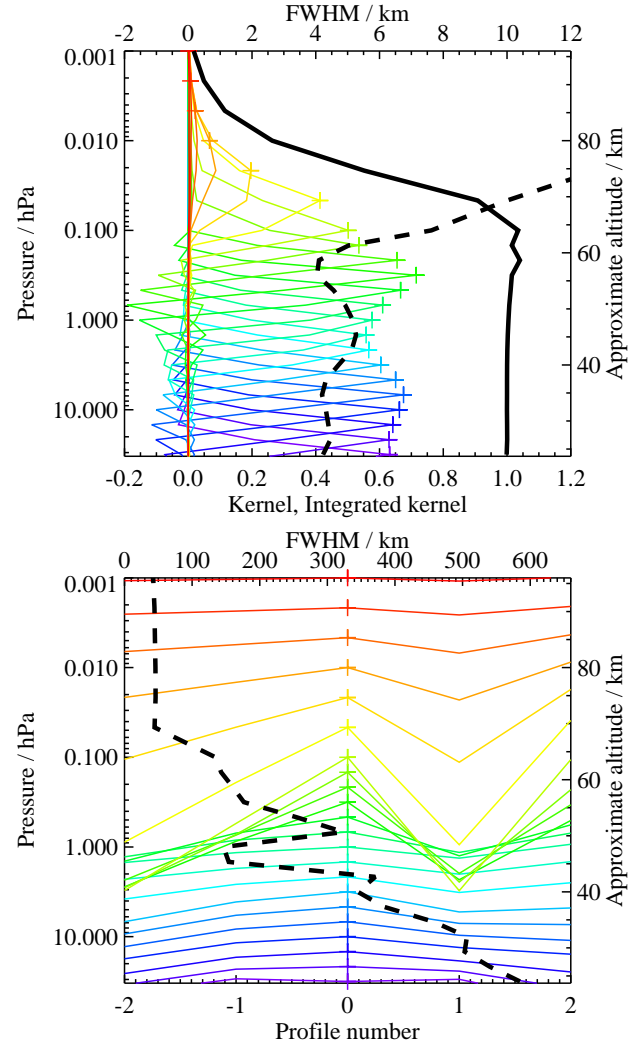


Figure 5. Averaging kernels for HO₂. See Figure 4 for further details.

the Doppler width at 1 hPa. At pressures below 1 hPa Doppler broadening is dominant and the peak intensity of OH spectral absorption is proportional to density. At pressures above 1 hPa, the peak intensity is proportional to vmr. The daytime OH density profile shows two peaks at ~ 45 km and ~ 75 km that are not as apparent in the vmr-based profiles. The night profile of OH exhibits the narrow layer at ~ 82 km that has been described earlier [Pickett *et al.*, 2006c]. Precisions are such that an OH zonal average with a 10° latitude bin can be determined with better than 10% relative precision with one day of data (100 samples) over 21–0.01 hPa. With 4 days of data, the 10% precision limits can be extended to 32–0.0046 hPa.

A typical HO₂ concentration profile and associated precision estimate is shown in Figure 7. The profile is shown both in volume mixing ratio (vmr) and density units. Precisions are such that a HO₂ zonal average with a 10° latitude bin can be determined with better than 10% relative precision from 20 days of data (2000 samples) over 21–0.032 hPa.

Expected Accuracy and Error characterization

A major component of the validation of MLS data is the quantification of the various sources of systematic uncertainty. Systematic uncertainties arise from instrumental issues: e.g., radiometric calibration, field of view characterization, spectroscopic uncertainty, and approximations in the retrieval formulation and implementation. This section summarizes the relevant results of a comprehensive quantification of these uncertainties that was performed for all MLS products. More information on this assessment is given in Appendix A of Read *et al.* (*this issue*) and repeated in the supplementary material of this paper.

The impact on MLS measurements of radiance (or pointing where appropriate) of each identified source of systematic uncertainty has been quantified and modeled. These modeled impacts correspond to either $2\text{-}\sigma$ estimates of uncertainties in the relevant parameters, or an estimate of their maximum reasonable errors based on instrument knowledge and/or design requirements. The effect of these perturbations on retrieved MLS products has been quantified for each source of uncertainty by one of two methods.

In the first method, sets of modeled errors corresponding to the possible magnitude of each uncertainty have been applied to simulated MLS cloud-free radiances, based on a model atmosphere, for a whole day of MLS observations. These sets of perturbed radiances have then been run through the routine MLS

data processing algorithms, and the differences between these runs and the results of the ‘unperturbed’ run have been used to quantify the systematic uncertainty in each case. The impact of the perturbations varies from product to product and among uncertainty sources. Although the term ‘systematic uncertainty’ is often associated with consistent additive and/or multiplicative biases, many sources of ‘systematic’ uncertainty in the MLS measurement system give rise to additional scatter in the products. For example, although an error in the O₃ spectroscopy is a bias on the fundamental parameter, it has an effect on the retrievals of species with weaker signals (e.g., HNO₃ that is dependent on the amount and morphology of atmospheric ozone). The extent to which such terms can be expected to average down is estimated to first order by these ‘full up studies’ through their separate consideration of the bias and scatter each source of uncertainty introduces into the data. The difference between the retrieved product in the unperturbed run and the original ‘truth’ model atmosphere is taken as a measure of uncertainties due to retrieval formulation and numerics.

In the second method, the potential impact of some remaining (typically small) systematic uncertainties has been quantified through calculations based on simplified models of the MLS measurement system (see Read *et al.*, *submitted*, 2007). Unlike the ‘full up studies’, these calculations only provide estimates of ‘gain uncertainty’ (i.e., possible multiplicative error) introduced by the source in question. This approach does not quantify possible biases or additional scatter for these minor sources of uncertainty.

Finally, although the MLS observations are unaffected by thin cirrus clouds or stratospheric aerosols, thick clouds associated with deep convection can have an impact on the MLS radiances. The MLS Level 2 data processing algorithms discard or downplay radiances identified (through comparison with predictions from a clear-sky model) as being strongly affected by clouds [Livesey *et al.*, 2006]. The contribution of cloud effects to the systematic uncertainty, both from the presence of clouds not thick enough to be screened out by the cloud filtering and from the loss of information through omission of cloud-impacted radiances, has been quantified by adding scattering from a representative cloud field to the simulated radiances and comparing retrievals based on these radiances to the unperturbed results. The cloud-induced effects shown in Figures 8 and 10 are estimated by considering only the cloudy profiles (as defined by the known amount of cloud in the ‘truth’ field). The contribution of clouds to HO_x systematic er-

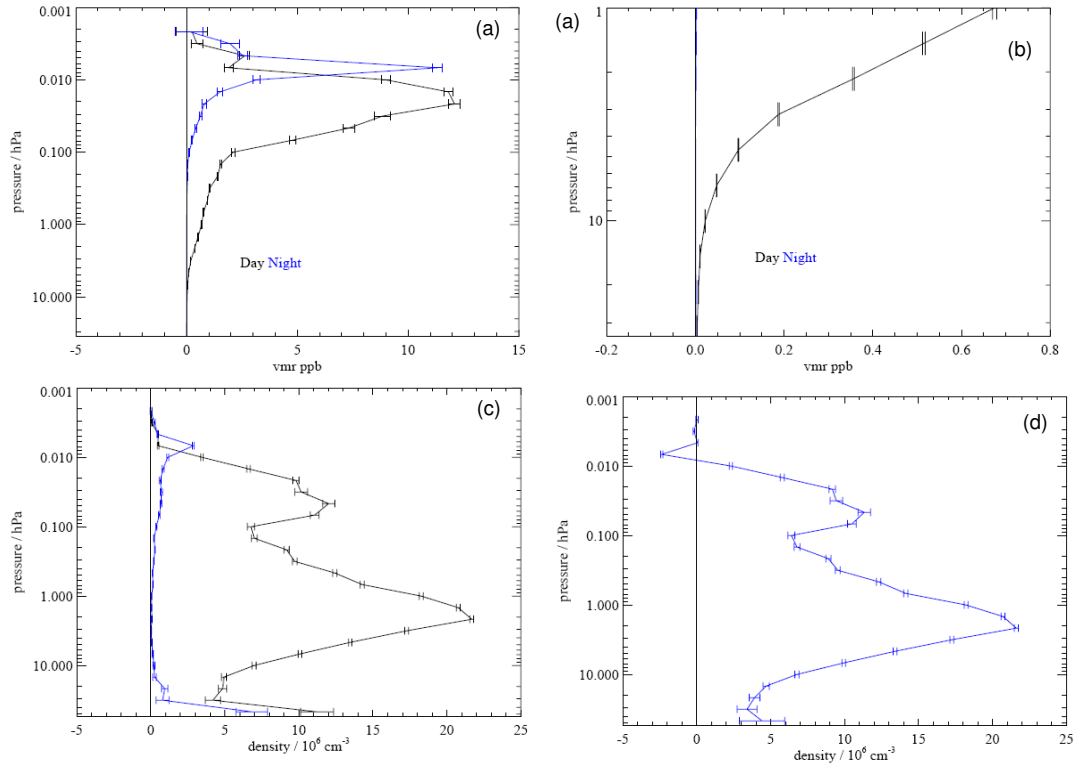


Figure 6. Zonal mean of retrieved OH and its estimated precision (horizontal error bars) for 20 September 2005 averaged over 29N to 39N. The average includes 368 profiles. Panel (a) shows vmr vs. pressure for day (black) and night (blue) overpasses. Panel (b) shows the same data plotted for the stratosphere. Panel (c) shows the same data converted to density units. Panel (d) shows the day–night differences for the data in panel (c).

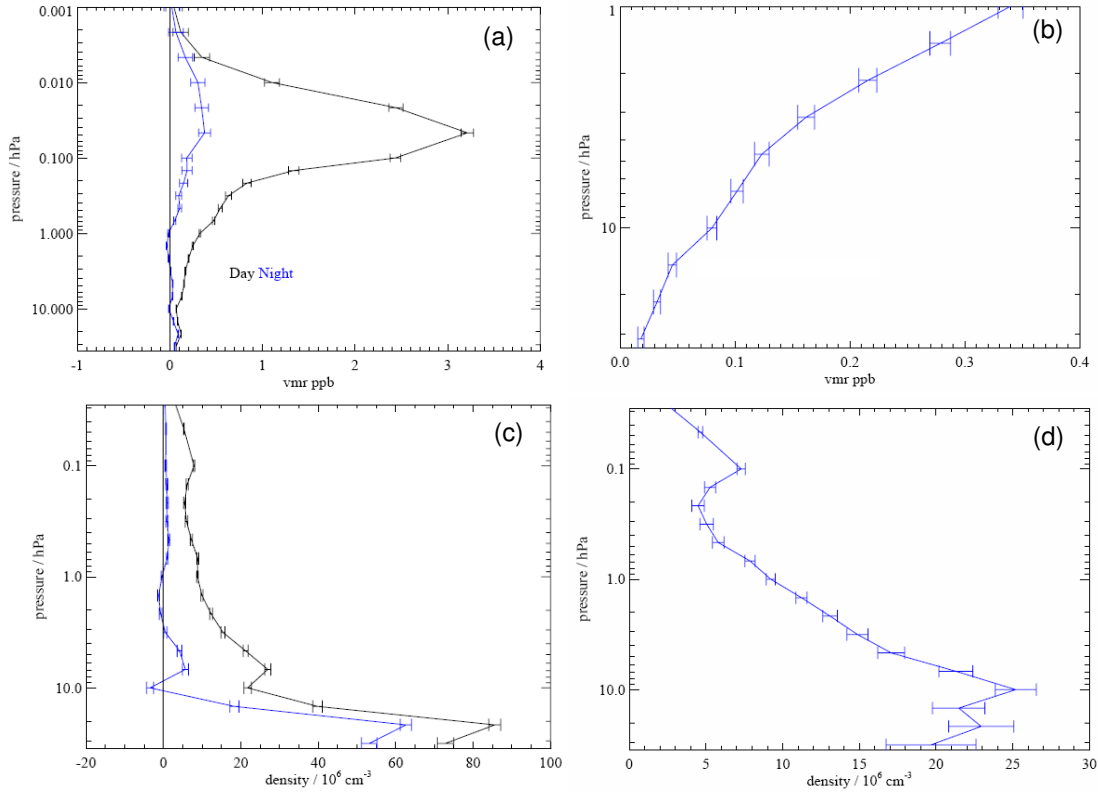


Figure 7. Zonal mean of retrieved HO₂ and its estimated precision for 20 September 2005 averaged over 29N to 39N. The average includes 2879 profiles. Panel (a) shows vmr vs. pressure for day (black) and night (blue) overpasses. Panel (b) shows the same data plotted as a day-night difference for the stratosphere. Panel (c) shows the same data converted to density units. Panel (d) shows the day-night differences for the data in panel (c).

rors is negligible in part because the high pressure limit of 31–22 hPa is much lower than the pressures expected for thick clouds. The thin polar mesospheric clouds are also not observable at MLS wavelengths.

The estimated impacts of the systematic errors on OH are summarized in Figure 8. The largest contributors to systematic bias errors contributing to the systematic bias errors is the radiometric and spectral calibration category. The two biggest contributors to this category are sideband fraction and gain compression and are approximately equal. The multiplicative errors are estimated to be less than 8% for pressures above 0.02 hPa. The dominant contributor to the slope error below 0.02 hPa is sideband fraction. The size of the OH errors relative to a typical profile can be seen by using a profile such as that in Figure 6.

An independent measure of the effect of sideband fraction uncertainty is to compare O₃ retrieved from the THz radiometer with that retrieved from the GHz radiometers. A comparison given by *Froidevaux et al. (this issue)* shows that the ratio of the O₃ concentrations is unity within 5% over 1–32 hPa. The uncertainty in OH due to sideband fraction should be the same as the uncertainty in the O₃(THz)/O₃(GHz) ratio. A complicating factor is that O₃(THz) line in bands 16 and 19 has a much stronger temperature dependence than O₃(GHz) lines. The calculated ratio of absorption coefficients changes by 1.7%/K, so the effect of temperature on the ozone ratio is small but not negligible. We therefore extend the low pressure boundary of the region with systematic errors that are < 8% to 0.03 hPa.

An independent view of the effect of a priori assumptions can be determined by synthetic calculations of radiance. It is important to have several measures of the contribution of a priori assumptions to the data. Figure 9 shows an example of such a calculation. Here the night a priori profile contributes 7% to the output data at 0.0068 hPa. The large daytime peak in the a priori at 0.03 hPa shows no impact on differences between the assumed profile and the retrieved profile and the amount of a priori mixing is even smaller than at higher altitudes.

The systematic errors on HO₂ retrieved concentration are summarized in Figure 10. The largest contributor of bias errors are sideband fraction and gain compression within the category of radiometric and spectral calibration. Again, the systematic errors from sideband fraction and gain compression are approximately equal. Both contribute to the low altitude peak in bias and standard deviation. The slope error has a peak at 10 hPa due to a priori and radiometric numerics (*Read*

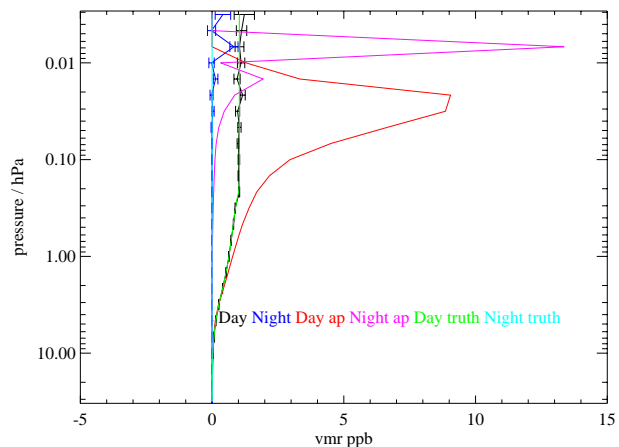


Figure 9. Retrieval results for synthetic OH profiles. The green line is the profile used to generate the synthetic daytime radiances. The red line is the daytime a priori profile. The black line with error bars is the retrieval output for the daytime profile and overlaps the green line. The error bars are the precision based on an estimated radiance uncertainty. No noise was added to the radiance. The night input profile (blue) was zero. The magenta line that peaks at 0.007 hPa is the night a priori profile. The blue line with error bars is the output retrieval for night.

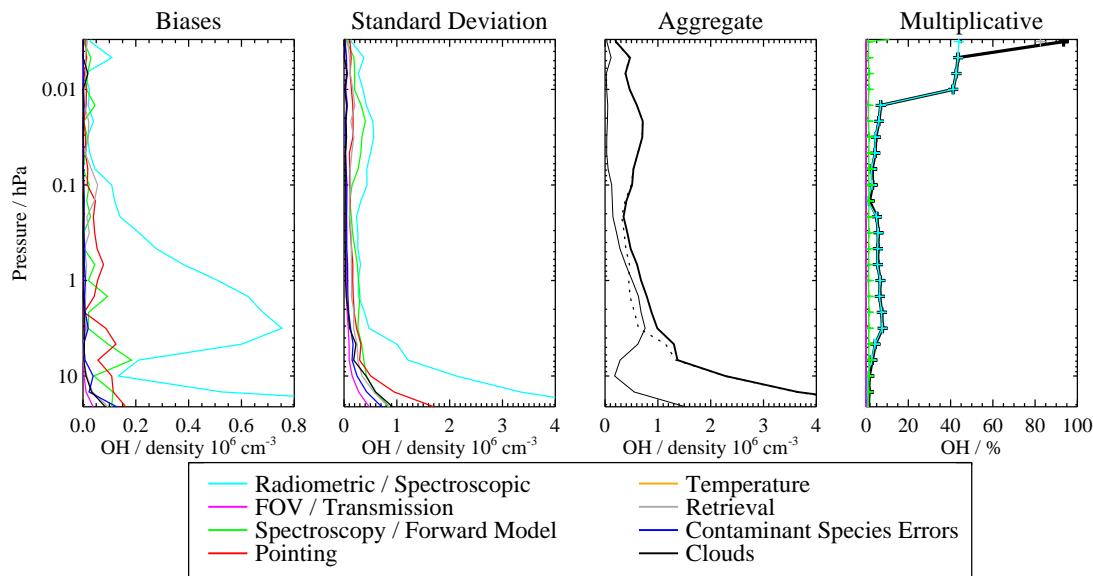


Figure 8. The estimated impact of various families of systematic errors on the MLS OH observations using day–night differences. The first two panels show the (left) possible biases that are independent of concentration and (center left) additional scatter introduced by the various families of errors, with each family denoted by a different colored line. (Right center) the root sum squares (RSS) of all the possible biases (thin solid line), all the additional scatters (thin dotted line), and the RSS sum of the two (thick solid line). The right panel shows errors that are proportional to the concentration.

et al., this issue). The slope error < 0.1 hPa is due to filter position uncertainty. The size of the HO₂ systematic errors relative to a typical profile can be seen using Figure 7.

The effect of a priori assumptions can also have an important effect on the HO₂ data. Figure 11 shows a retrieval that uses synthetic radiance derived from an input profile that is constant above 0.1 hPa. The a priori concentration profile is zero throughout. The retrieval tracks the input profile below 0.1 hPa. For pressures below 0.032 hPa there is at least 20% a priori contamination.

Differences between software versions v2.2 and v1.5

For the THz radiometer data in v2.2, the first step for level-1 calibration of MLS emission is to calibrate the data using a procedure that is a slight modification from the calibration described in Pickett [2006a] for v1.5. The need for calibration change was found by examining the on-orbit variation of gain as a function of orbital phase. The gain has an approximately sinusoidal dependence on orbital phase that is 2 to 4% of the average value with a magnitude that depends on

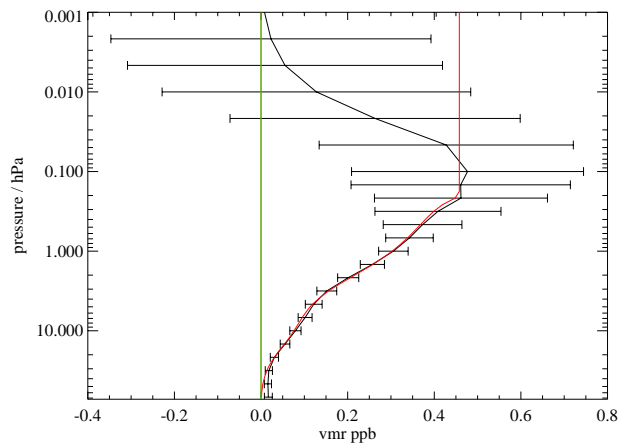


Figure 11. Retrieval results for synthetic HO₂ profiles. The red line is the profile used to generate the synthetic radiances. The black line is the retrieval output. The green line at zero is the a priori profile. The error bars are the precision based on a theoretical estimated radiance uncertainty. No noise was added to the radiance.

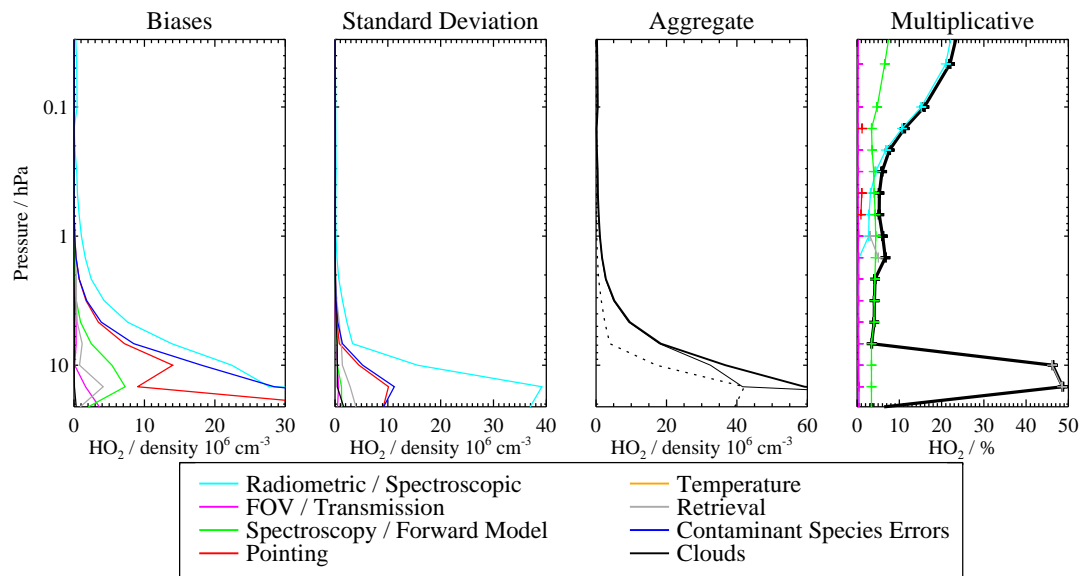


Figure 10. The estimated impact of various families of systematic errors on the MLS HO₂ observations of day–night differences. The first two panels show the (left) possible biases and (center) additional scatter introduced by the various families of errors, with each family denoted by a different colored line. For further details, see Figure 8

the filter channel. The gain change is needed to account for small thermal effects on gain over the orbit. In v1.5, the gain was assumed to be constant over the orbit. In v2.2, the fitted gain is now assumed to have an additional sinusoidal dependence on orbital phase as well as the constant dependence assumed in v1.5. The second change in v2.2 calibration is that the radiometric zero is derived only from the space view, whereas before in v1.5 it was derived from both the space view and the calibration target. This change makes small radiances less sensitive to assumptions about the gain. Both changes are part of v2.2 level 1 processing. The result is that the OH radiance has better calibration, improving accuracy by as much as 2%.

In the OH v1.5 retrieval, the profiles were fitted to a pressure level interval of 3/decade below 0.1 hPa and 6/decade at higher pressures. In v2.2 the profile sampling is 6/decade over the whole pressure range. There are many beneficial changes in OH above 50 km as can be seen in Figure 12. The profiles are smoother, have uniform pressure resolution, and have much fewer instances of negative concentration. In the stratosphere, OH fits are less subject to convergence problems in part because the iteration limit has been increased from 4 to 6.

The main change for HO₂ is that there is more smoothing applied in version 2.2. In v1.5, no effective

smoothing was applied and the profiles tended to have a small but significant oscillation in concentration with height. This kind of behavior is often an indication that the retrieval fitting is almost indeterminant, and the smoothing in v2.2 is effective in reducing this problem. The effect of smoothing at altitudes below 60 km is to broaden the averaging kernel to 4 km FWHM in the vertical and as much as 6 degrees along the track. Because of smoothing, precisions are no longer flagged negative above 60 km (0.1 hPa). However, it is estimated that there is at least 20% a priori contamination for pressures below 0.032 hPa (see above).

The second change for v2.2 was to set the HO₂ a priori concentration to zero. The v1.5 HO₂ a priori concentrations were based on the results of model calculations. This change was made to avoid potential artifacts in smoothing due to the a priori assumptions. With zero a priori HO₂ and finite a priori uncertainty, the effect of a priori assumptions will be to lower the retrieved HO₂ relative to truth.

Comparisons with other Data Sources

Comparison with Balloon-borne Instruments

Aura MLS validation campaigns took place in Sept 2004, 2005 involving balloon-borne instruments flown from Ft. Sumner, NM (latitude = 34.5° and longitude

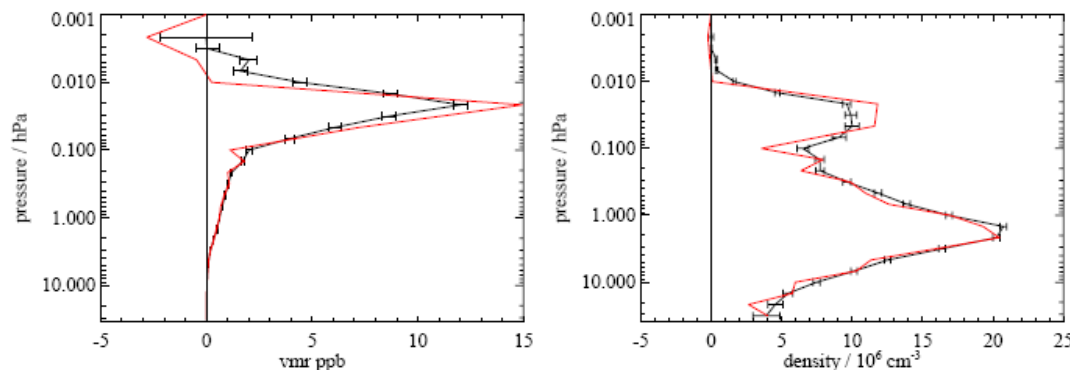


Figure 12. Comparison between v1.5 and v2.2 for MLS OH for September 23, 2004 zonally averaged over 29–39°N latitude. Red is version v1.5 and black is version v2.2. The same data is plotted in vmr (left panel) and density (right)

= -104°). The Balloon OH instrument (BOH) and the Far Infrared Spectrometer (FIRS-2) instrument were launched on a common balloon gondola on September 23, 2004. Details of the 2004 flight can be found in *Pickett et al.* [2006b]. During the 2005 flight, the Submillimeter Limb Sounder (SLS) accompanied the BOH and FIRS-2 instruments. The balloon stayed aloft at ~38 km for nearly 24 hours for this flight. The results of all these measurements are summarized in Figure 13 along with a calculated profile from a photochemical model.

The MLS OH profiles are a zonal mean over 29–39°N latitude. The MLS HO₂ profiles for 2004 are a zonal mean over latitudes < 50°. The mean solar zenith angle (42°) was close to the solar zenith angle at the time of the closest overpass (39°). The MLS HO₂ profiles for 2005 are a zonal mean over 24–44°N latitude for 9 days centered on the day of the balloon flight.

The BOH instrument is a heterodyne limb-viewing thermal emission instrument that is functionally identical to the THz module on MLS [*Pickett*, 2006b] and only measures OH. The FIRS-2 instrument is a thermal emission far-infrared Fourier transform spectrometer developed at the Smithsonian Astrophysical Observatory [*Jucks et al.*, 1998]. It measures OH and HO₂ in the far infrared using multiple lines. SLS [*Stachnik et al.*, 1992] is a cryogenic heterodyne instrument that measures atmospheric radiance in the same spectral region as the MLS 640 GHz region. One of the molecules measured by SLS is HO₂. The balloon instruments all use limb sounding to increase the effective path length. However, there is only an increase for tangent heights below the balloon altitude. The path lengths for layers

above the balloon are an order of magnitude smaller than at the tangent height. Accordingly, the balloon instruments have only 1-2 independent pieces of information above the balloon. The dotted lines for the profiles in Figure 13 show the assumed OH distribution that was used for each of the balloon retrievals. In all cases, the error bars are 1- σ total error (precision and accuracy).

Pickett et al., [2006b] reported good agreement (within 17% over 25–40 km) between the 2004 balloon and satellite observations of OH from 25–40 km. Observations of HO₂ agreed within 23% below 40 km.

Here, the Sept. 2004 comparisons have been updated using the v2.2 MLS retrievals and a current version of the photochemical model, Mdl_C06 (see below), that incorporates JPL 2006 kinetics [*Sander et al.*, 2006]. Furthermore, this analysis has been extended to the 2005 observations. Figure 13 (top left) compares the new MLS OH retrieval for 2004 to the FIRS-2 and BOH measurements. Compared to the previously published comparisons, there is better agreement (within 15%) between balloon observations of OH and the new MLS retrievals. The oscillations in the MLS HO₂ profile reported by *Pickett et al.*, [2006b] are notably absent in the updated version (Figure 13, top right). Also, the error bars shown reflect the formulation for instrument precision described above. The agreement between HO₂ observations has improved to within 18%.

The HO₂ measurements overlap with the two balloon measurements within a combined experimental error of 20%. The precision for day–night differences has been multiplied by 3^{1/2} to account for the effects of the width of the horizontal averaging kernel (3 scans). There is

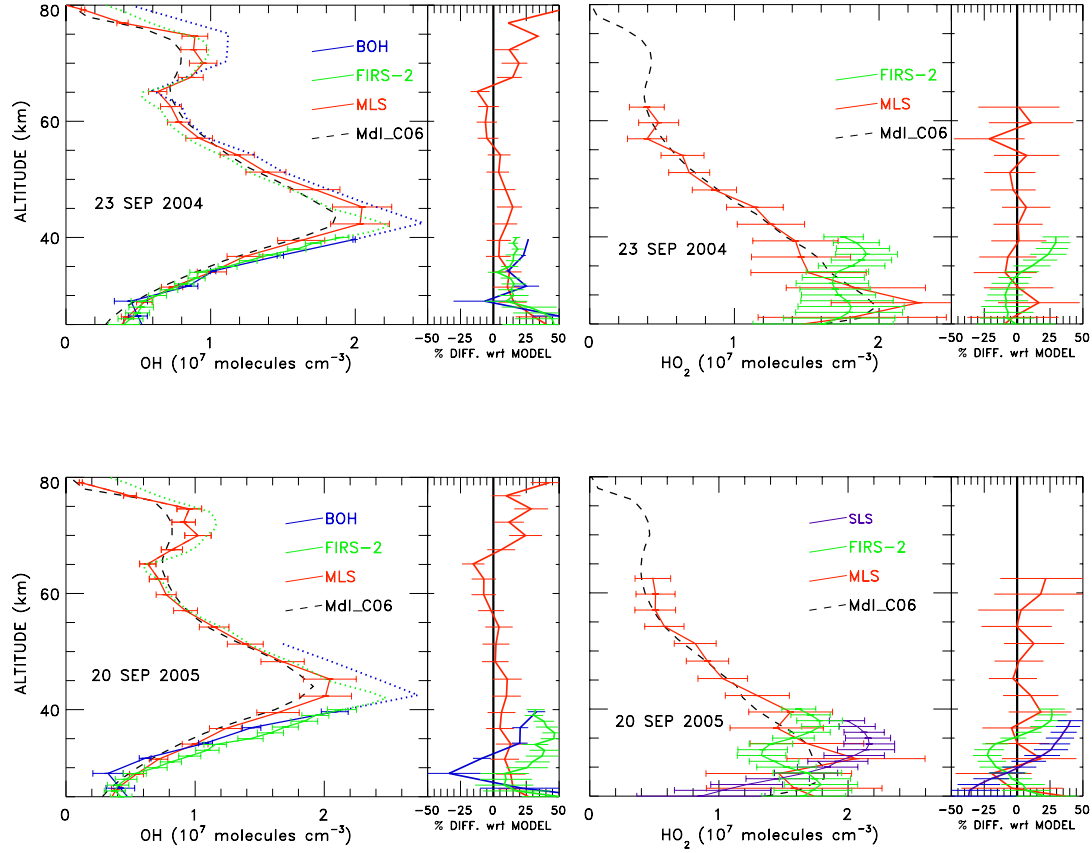


Figure 13. Balloon-borne HO_x observations for 23 September 2004 and 20 September 2005 near Ft. Sumner, NM, USA. The top panel uses a zonal mean of MLS OH over a latitude range of 29–30°. The bottom panel uses a 9-day zonal mean of MLS HO₂ over the same latitude interval. The balloon-borne instrument profiles above 40 km are shown as dotted lines to indicate the assumed profile. The balloon data and model calculations are for the time of the MLS overpass.

no evidence that multiplicative systematic errors are as large as is shown in Figure 10. However, significant differences in HO₂ exist among the three instruments (Figure 13, lower right). From 30–35 km the FIRS-2 and SLS instruments disagree by as much as 34%. The reason for this discrepancy is unclear at this time.

The same comparisons for the 2004 validation campaign are carried out for the Sept 2005 flights. The agreement among OH observations is $\pm 18\%$ (Figure 13, bottom left). However, the peaks in OH inferred from the OH partial column above float measured by FIRS-2 (2.5×10^7 molecules cm^{-3}) and BOH (2.7×10^7 molecules cm^{-3}) are larger than the peak observed by MLS (2.0×10^7 molecules cm^{-3}) and outside of the MLS error bars. The MLS HO₂ measurements overlap with the two balloon measurements within a combined experimental error of 20%. However, there are significant differences between FIRS-2 and SLS from 30–35 km which need further study. There is no evidence that multiplicative systematic errors are as large as is shown in Figure 10. Figure 13 shows that MLS and the model agree within the MLS precision.

The study by *Canty et al.* [2006] compared model results that tested combinations of kinetics parameters to the observations from 2004. They determined that best agreement was found between the MLS observations of OH, HO₂, OH/HO₂, and HO_x and a model using JPL 2002 kinetics [Sander et al., 2003], the rate for O+OH suggested by *Smith and Stewart* [1994], and a 20% increase in OH+HO₂ (denoted Mdl_C or Mdl_C02). These changes in the two rates are within their assigned uncertainty, but give improvements in the agreement between the model and earlier MLS results. Mdl_C06 uses the same modification of the two reaction rates without further adjustment, but incorporates JPL 2006 kinetics [Sander et al., 2006]. The model is constrained to MLS observations of H₂O, O₃, N₂O, CO, and temperature appropriate to the dates of each validation campaign. Methane and nitric acid are inferred from N₂O through tracer relationships. The reduced chi square (χ^2_r) values between MLS observations and model for 2004 and 2005 are shown in Figure 14. A χ^2_r value of unity or less indicate model results within the experimental error. Results for both years are presented for MLS v1.5 and Mdl_C02 (black bars) and MLS v2.2 and Mdl_C06 (blue bars). There is overall improved agreement between model and observations for both days, primarily due to updated HO₂ retrievals, which are averaged more than the previous version, and the better formulation for the precision associated with these observations. It should be emphasized that the

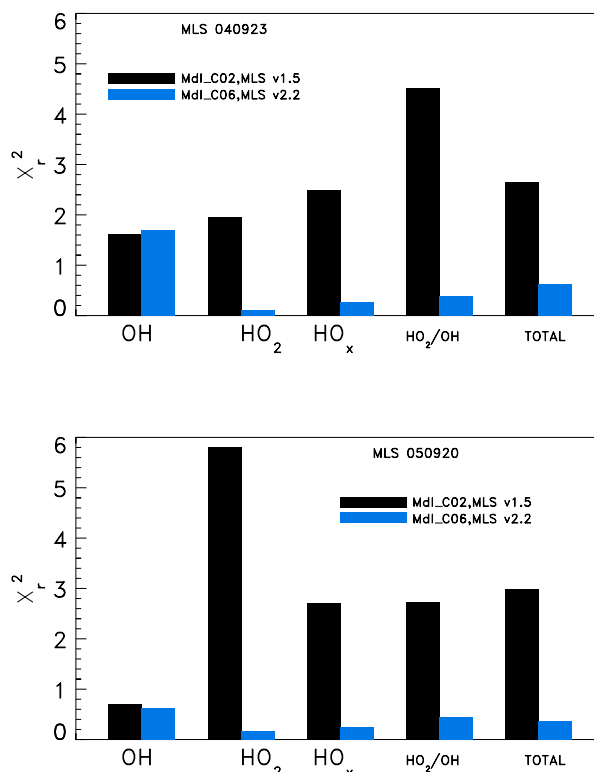


Figure 14. Comparison between model and MLS OH and HO₂ for 23 September 2004 and 20 September 2005. Black bars are v1.5 retrievals and blue bars are v2.2

two rate constant adjustments were not reoptimized between Mdl_C02 and Mdl_C06. In addition, MLS v1.51 was used by [Canty et al., 2006] and MLS v2.2 is used here.

Comparison with Ground-based Column Measurements

At the time of the September 23, 2004 balloon flight, both the Poly-Etalon Pressure Scanned Interferometric Optical Spectrometer (PEPSIOS) instrument [Minschwaner et al, 2003] and the Fourier Transform Ultraviolet Spectrometer (FTUVS) instrument [Cageao, et al., 2001] were observing the OH column in absorption against the Sun at 308 nm. The PEPSIOS instrument was located in Socorro, New Mexico, USA (34°N, 107°W) and the FTUVS was located at Table Mountain, California, USA (34.5°N, 117.7°W). The observations are shown in Figure 15. The model in the dashed line is Mdl_C06 described above. The solid line is JPL06 rate constants [Sander, et al., 2006] with no modification. BOH, FIRS-2, and MLS were corrected

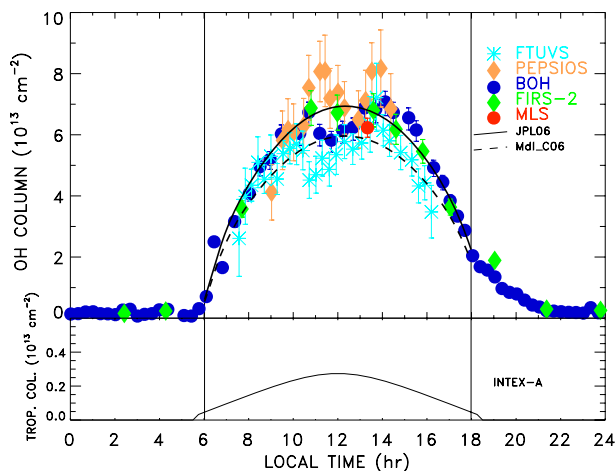


Figure 15. Comparison of OH columns for September 23, 2004. The lower panel shows the total tropospheric correction to the balloon-borne and MLS stratospheric and mesospheric column. The upper panel shows these measurements along with the column from two ground-based instruments. Two versions of the model are also shown.

by adding both a tropospheric column using data of Wennberg *et al* [1998] and an additional contribution from the boundary layer [Singh *et al.*, 2006]. The contribution from both these two sources of tropospheric OH is 7% of the total column. Both sources make similar contributions to the column. See the Appendix for further details.

As before, the agreement between different column measurements is within most error estimates. PEPSIOS observations are generally higher than the FTUVS observations, especially at high sun. While the contribution to the total column from the troposphere is believed to be small ($\sim 5\%$), it should be noted that the FTUVS instrument generally lies above the boundary layer and will therefore receive no contribution to the total column from this region of the atmosphere. The PEPSIOS/FTUVS differences are larger than the expected contribution of boundary layer OH to the total column, and hence unlikely to be the explanation.

As with the balloon-based measurements, the agreement between different column measurement is close, but significant differences between instruments may exist. The column can be a sensitive measure of OH in the stratosphere and mesosphere. Figure 16 shows the fractional contribution to the OH column for different altitude intervals. These fractions were determined from the actual MLS profile for September 23, 2004

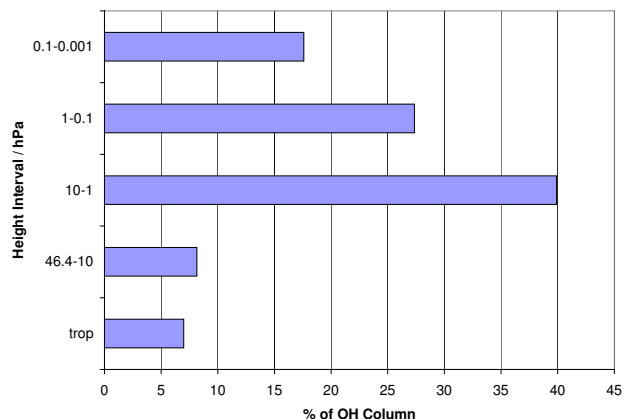


Figure 16. Contribution of different height intervals to the total OH column.

above 20 km, modeled OH for 12–21 hPa, and the estimated contributions from the mesosphere and boundary layer. The mesospheric portion (and associated slow chemistry) is responsible for morning–afternoon asymmetries, while the largest contribution comes from the upper stratosphere near the 45 km peak in density. The MLS OH column for this day has increased in v2.2 by 9% compared to v1.5 due to improvements in the MLS mesospheric OH.

Comparison with MAHRSI

The Middle Atmosphere High Resolution Spectrograph Investigation (MAHRSI) instrument flew on the Space Shuttle in 1994 [Conway *et al.*, 1999] and 1997 [Conway *et al.*, 2000]. We focus on the more recent flight because the observations were made at lower solar zenith angles (SZA) where the OH concentration is higher. We compare the MAHRSI data for August 15, 1997 with a zonal average of MLS data for September 7, 2005 over latitude range of 12–32°S and 33–53°N. This latitude range for the MLS zonal average was selected so that the SZA matched the MAHRSI range (32–49°). The comparison is shown in Figure 17. The MAHRSI points are median values for a given altitude range. The error bars for MLS and MAHRSI OH include precision and systematic errors (2σ root sum of squares). The 2σ uncertainties nearly overlap, but there are correlations in height. A 10 km box-car average would not overlap nearly as well. It is probabilistically unlikely that the two observations truly agree. At the 42 km OH peak the MAHRSI value is 50% higher than MLS, and at the 70 km OH peak the MAHRSI values are 20% lower than MLS. Below 50 km, the MAHRSI mea-

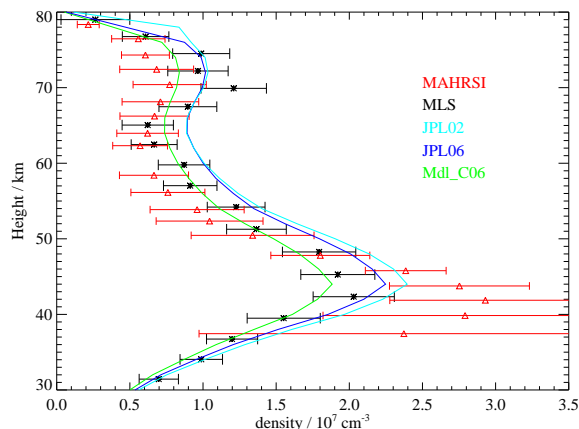


Figure 17. MLS OH altitude profiles compared with MAHRSI. The black line with error bars is a zonal average of OH profiles from MLS for September 7, 2005. The MAHRSI median data for August 15, 1997 is denoted by red triangles. The error bars for MLS and MAHRSI OH include precision and systematic errors (2σ). The latitude range ($12\text{--}32^\circ\text{S}$, $33\text{--}53^\circ\text{N}$) for the MLS zonal average was chosen so that the SZA range matches the MAHRSI SZA range ($32\text{--}49^\circ$). Model results for JPL02 (blue line), JPL06 (black line) and Model C06 (green line) are also shown.

measurements are challenging due to absorption of the OH signal by O₃ at 300 nm wavelength. This systematic error is reflected in the uncertainties.

Figure 17 also shows the results of three model simulations: JPL02, JPL06, and Mdl_C06. The models were constrained to MLS observations of H₂O, O₃, N₂O, CO, and temperature that were averaged over the same latitude range as was used for the MLS OH observations. The JPL06 photochemical model using standard chemistry (i.e., recommended rate constants) is in good agreement with MLS over 30–80 km except that MLS has a more pronounced minimum at 63 km. The simulation using JPL06 kinetics results in slightly lower abundances of OH than the JPL02 simulation because of changes to the rate constants for O(¹D) quenching and the new recommendation for temperature dependencies of O(¹D)+H₂O. Results are also shown for Mdl_C06 (defined above), which follows from the work of *Canty et al.* [2006] (this earlier paper was based on version 1.5 MLS data and was completed before the JPL06 recommendation was released). Similar to *Canty et al.* [2006], we find the perturbations to the rate constants for O+OH and OH+HO₂ that constitute Mdl_C06 re-

sult in overall excellent agreement between measured and modeled OH and HO₂ at all altitudes (Figure 14) and a model profile for OH that falls within the MLS measurement uncertainty at all altitudes.

The shape of the MLS version 2.2 OH profile is simulated well using standard chemistry. This conclusion is consistent with statements in Pickett et al. [2006] and Canty et al. [2006], based on version 1.5 MLS data, that the MLS measurements of OH and HO₂ are not consistent with the so-called “HOx dilemma” that resulted from analysis of the MAHRSI observations [Conway et al., 2000 and Summers et al., 1997]. We consider it unlikely that changes in H₂O and O₃ between August 15, 1997 and the time of the MLS observations can account for the different shapes of the OH profile measured by the two instruments. This statement is supported by the fact that *Jucks et al.* [1998] were able to reproduce the model results of *Summers et al.* [1997] using the profiles of H₂O and OH that were used to interpret the MAHRSI data. Our group has consistently found reasonably good agreement between measured and modeled profiles of OH and we find no evidence for secular changes in H₂O and OH above 40 km that would be large enough to account for a shift in OH between 1997 and 2005, that is anywhere near the magnitude of the difference between MAHRSI and MLS OH at 40–80 km altitude.

Summary and Conclusions

Version v2.2 is a substantial improvement from v1.5 particularly for mesospheric OH and stratospheric HO₂. Use of v1.5 HO₂ products can benefit from user-applied smoothing, but the internal smoothing in v2.2 is to be preferred because the averaging is done during the retrieval fit. OH in the upper stratosphere is very similar for the two versions.

A summary of the analysis of systematic errors is shown in Table 3 for OH and in Table 4 for HO₂. For OH, use of day–night differences are recommended for OH at pressures ≥ 10 hPa because the bias uncertainty becomes zero when the differences are taken. The slope or scaling uncertainty for OH is $<8\%$ for pressures > 0.003 hPa if due regard is taken of the consistency of THz O₃ measurements as discussed above. Day–night differencing is not needed near 1 hPa because the bias is 0.3% of typical daytime OH densities. In addition, observed night concentrations of OH for 10–0.1 hPa are $<1\%$ of noontime tropical values. Use of day–night differences is recommended for HO₂ over the entire usable range of 21–0.03 hPa. The scaling errors for HO₂

Table 3. Summary of precisions, resolution, and uncertainties for the MLS OH product

Region	Resolution		Bias uncertainty / 10 ⁶ cm ⁻³
	Vert. / km	Horiz. / km	
<0.003 hPa	—	—	—
0.003 hPa	5.0 × 220	—	0.034
0.01 hPa	2.5 × 200	—	0.031
0.1 hPa	2.5 × 180	—	0.12
1.0 hPa	2.5 × 165	—	0.50
10 hPa	2.5 × 165	—	0.18
32–10 hPa	2.5 × 165	—	0.50
1000–32 hPa	—	—	—

^a Precision on individual profile

are estimated to be larger, as much as 46% at 10 hPa. However, comparison with balloon measurements show that the actual systematic bias for HO₂ at 10 hPa is < 20%. Comparisons for both OH and HO₂ balloon measurements, models, and MLS measurements show good agreement, as do the column measurements.

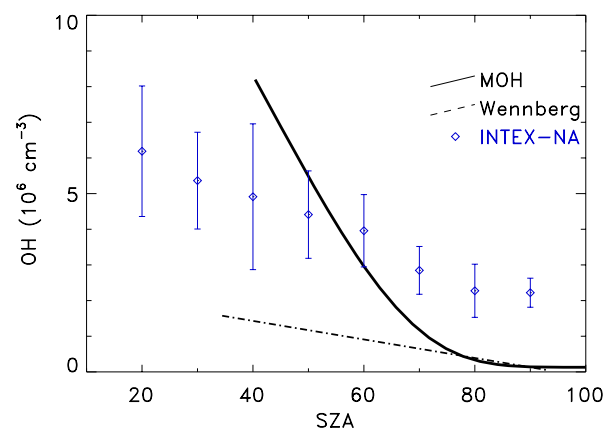
Further work is needed to understand remaining differences among MLS measurements, and balloon instruments, the column measurements of OH, and MAHRSI. In all cases the 2- σ uncertainty nearly overlaps, but there are differences that are unexplained and significant. The results for Mdl_C06 fall very close to the data, even though the model was not re-optimized for the v2.2 MLS data. The model calculation shows that standard chemistry, with slightly modified rates, is consistent with measured stratospheric and mesospheric MLS HO_x. This conclusion is consistent with *Canty et al.* [2006], but here we use MLS v2.2 data and kinetics based on JPL 2006 rates. While there are still large uncertainties in the measurements, MLS HO_x observations do not require new reactions or new rates that differ from recommended values by more than their estimated uncertainties. In this sense, we no longer perceive that there is a “HO_x dilemma.”

Appendix

The amount of OH in the free troposphere and boundary layer is approximated by the use of aircraft measurements (Figure 18). Observations of OH taken in the upper troposphere during August 1996 near Hawaii [*Wennberg et al.*, 1998] and the boundary layer region during the INTEX-NA campaign from July - August 2004 in the north eastern US [*Singh et al.*, 2006] are shown. We present here additional boundary

Table 4. Summary of precisions, resolution, and uncertainties for the MLS HO₂ product

Region	Resolution		Bias uncertainty / 10 ⁶ cm ⁻³	Scaling uncertainty / %
	Vert. / km	Horiz. / km		
< 0.03 hPa	Unsuitable for scientific use	Unsuitable for scientific use	—	—
0.03–0.1 hPa	16 × 600	—	0.39	22
0.1–1 hPa	16 × 400	—	0.46	10
1–10 hPa	5.5 × 660	—	1.1	6
10–100 hPa	4.5 × 450	—	37.	20
1000–10 hPa	—	—	—	—

^a Precision on individual profile difference
Unsuitable for scientific use**Figure 18.** Tropospheric OH vs. solar zenith angle

layer observations of OH using chemical ionization mass spectrometry taken during 1999–2003 from Meteorological Observatory Hohenpeissenberg (MOH), Germany [*Rohrer and Berresheim*, 2006] to illustrate the variation in measured OH between locations. The polynomial fits to the data taken from Hawaii and Germany are shown (solid and dashed-dotted curves, respectively). The mean and standard deviation of the INTEX-NA data are indicated by blue diamonds and blue lines. The higher values of OH in the boundary layer from the MOH site may be due to ozone rich air during the warm summer, whereas the lower OH values from Hawaii was seen in the colder upper troposphere.

Soundings from the National Weather Service in Albuquerque, NM indicate a boundary layer height of no more than 1.5 km. The INTEX-NA OH data are added to the total column assuming this boundary layer height. The *Wennberg et al.*, [1998] values of OH are included from the top of the boundary layer to the lowest level of the balloon observations (12 km) (Figure

15, bottom panel). The use of the MOH measurements, rather than those from INTEX-NA, lead to a very small increase in total column (not shown). If MOH had been the correct values to use, the maximum amount of OH added to the column would be $3.4 \times 10^{12} \text{ cm}^{-3}$, a change in tropospheric contribution of less than 1%.

Acknowledgments. We wish to thank all who helped make the Aura HO_x measurements possible. Thanks to the Aura Project for their support throughout the years (before and after Aura launch), in particular M. Schoeberl, A. Douglass (also as co-chair of the Aura validation working group), E. Hilsenrath, and J. Joiner. We also acknowledge the support from NASA Headquarters, P. DeCola for MLS and Aura, and M. Kurylo, J. Gleason, B. Doddridge, and H. Maring, especially in relation to the Aura validation activities and campaign planning efforts. We are grateful to the Columbia Scientific Balloon Facility for launch services. Research at the Jet Propulsion Laboratory, California Institute of Technology, is performed under contract with the National Aeronautics and Space Administration.

References

- Blake, G. A., J. Farhoomand, and H. M. Pickett (1986), The Far-infrared Rotational Spectrum of X²Π OH, *J. Mol. Spec.*, **115**, 226-228.
- Cageao, R. P., J. F. Blavier, J. P. McGuire, Y. B. Jiang, V. Nemtchinov, F. P. Mills, and S. P. Sander (2001), High-resolution Fourier-transform ultraviolet-visible spectrometer for the measurement of atmospheric trace species: application to OH Source, *Applied Optics*, **40**, 2024-2030.
- Canty, T., H. M. Pickett, R. J. Salawitch, K. W. Jucks, W. A. Traub, J. W. Waters (2006), Stratospheric and mesospheric HO_x: results from Aura MLS and FIRS-2, *Geophys. Res. Lett.*, **33**, L12802.
- Conway, R. R. *et al.* (1999), Middle Atmosphere High Resolution Spectrograph Investigation, *J. Geophys. Res. D*, **104**, 16327-16348.
- Conway, R. R. *et al.* (2000), Satellite Observations of Upper Stratospheric and Mesospheric OH: The HO_x Dilemma, *Geophys. Res. Lett.*, **27**, 2613-2616.
- Froidevaux, L. *et al.* (2006), Early Validation Analyses of Atmospheric Profiles from EOS MLS on the Aura Satellite, *IEEE Trans. Geosci. Remote Sensing*, **44**, 1106-1121.
- Jucks, K. W. *et al.* (1998), Observations of OH, HO₂, H₂O, and O₃ in the upper stratosphere: implications for HO_x photochemistry, *Geophys. Res. Lett.*, **25**(21), 3935-3938.
- Li, K.-F., R. P. Cageao, E. M. Karpilovsky, F. P. Mills, Y. L. Yung, J. S. Margolis, and S. P. Sander (2005), OH column abundance over Table Mountain Facility, California,: AM-PM diurnal asymmetry, *Geophys. Res. Lett.*, **32**, L13813, doi:10.1029/2005GL022521.
- Livesey, N.J., W.V. Snyder, W.G. Read, and P.A. Wagner (2006), Retrieval algorithms for the EOS Microwave Limb Sounder (MLS) instrument, *IEEE Trans. Geosci. Remote Sensing* **44**, 1144-1155.
- Minschwaner K., T. Canty, C. R. Burnett (2003), Hydroxyl column abundance measurements: PEPSIOS instrumentation at the Fritz Peak Observatory and data analysis techniques, *J. Atmos. Solar-Terrest. Phys.* **65**, 335-344
- Mueller, E. R. *et al.* (2007), Therahertz local oscillator for the Microwave Limbsounder on the Aura Satellite, *Appl. Optics*, **46**, 4907-4915.
- Osterman, G. B. *et al.* (1997), Balloon-borne measurements of stratospheric radicals and their precursors: Implications for the production and Loss of ozone, *Geophys. Res. Lett.*, **24**, L1107-L1110.
- Pickett, H. M. (2006a), Microwave Limb Sounder THz Module on Aura, *IEEE Trans. Geosci. Remote Sensing*, **44**, 1122-1130.
- Pickett, H. M. *et al.* (2006b), Validation of Aura MLS HO_x measurements with remote-sensing balloon instruments, *Geophys. Res. Lett.*, **33**, L01808-L01811.
- Pickett, H. M., W. G. Read, K. K. Lee, and Y. L. Yung (2006c), Observation of night OH in the mesosphere, *Geophys. Res. Lett.*, **33**, L19808.
- Rohrer, R., and H. Berresheim (2006), Strong correlation between levels of tropospheric hydroxyls and solar ultraviolet radiation, *Nature*, **442**, 184-187.
- Salawitch, R. J., *et al.* (2005), Sensitivity of ozone to bromine in the lower stratosphere, *Geophys. Res. Lett.*, **32**, L05811.
- Sander, S.P., *et al.* (2003) Chemical kinetics and photochemical data for use in atmospheric studies, evaluation number 14, *JPL Publ.*, 02-25.
- Sander, S.P., *et al.* (2006) Chemical kinetics and photochemical data for use in atmospheric studies, evaluation number 15, *JPL Publ.*, 06-2.
- Singh, H.B., *et al.* (2006) Overview of the summer 2004 Intercontinental Chemical Transport Experiment-North America (INTEX-A), *J. Geophys. Res.*, **111**, D24S01., doi:10.1029/2006JD007905.
- Smith, I.W.M., and D.W.A. Stewart (1994), Low temperature kinetics of reactions between neutral free radicals, Rate constants for the reactions of OH radicals with N atoms ($103 \leq T/K \leq 294$) and with O

- atoms ($158 \leq T/K \leq 294$), *J. Chem. Soc. Faraday Trans.*, *90*, 3221-3227.
- Summers, M. E., et al. (1997), Implications of satellite OH observations for middle atmospheric H₂O and ozone, *Science*, *277*, 1967.
- Stachnik, R. A., J. C. Hardy, J. A. Tarsala, J. W. Waters, and N. R. Erickson (1992), Submillimeter Wave Heterodyne Measurements of Stratospheric ClO, HCl, O₃, and HO₂ - 1St Results, *Geophys. Res. Lett.*, *19*, 1931-1934.
- Waters, J. W., et al. (2006), The Earth Observing System Microwave Limb Sounder (EOS MLS) on the Aura Satellite, *IEEE Trans. Geosci. Remote Sensing*, *44*, 1075-1092.
- Wennberg, et al. (1998), Hydrogen Radicals, Nitrogen Radicals, and the Production of O₃ in the Upper Troposphere, *Science*, *279*, 49-53.
-
- Herbert M. Pickett, B. J. Drouin, T. Canty, R. J. Salawitch, R. A. Fuller, V. S. Perun, N. J. Livesey, J. W. Waters, R. A. Stachnik, S. P. Sander, and W. A. Traub, Jet Propulsion Laboratory, 4800 Oak Grove Drive, Pasadena, CA 91109, USA. (herbert.m.pickett@jpl.nasa.gov)
- K. W. Jucks, Harvard-Smithsonian Center for Astrophysics, 60 Garden St., Cambridge, MA 02138, USA.
- K. Minschwaner, New Mexico Institute of Mining and Technology, Socorro, NM 87801, USA.